Volume 16
Number 34
14 September 2020
Pages 7879–8086

Soft Matter

rsc.li/soft-matter-journal

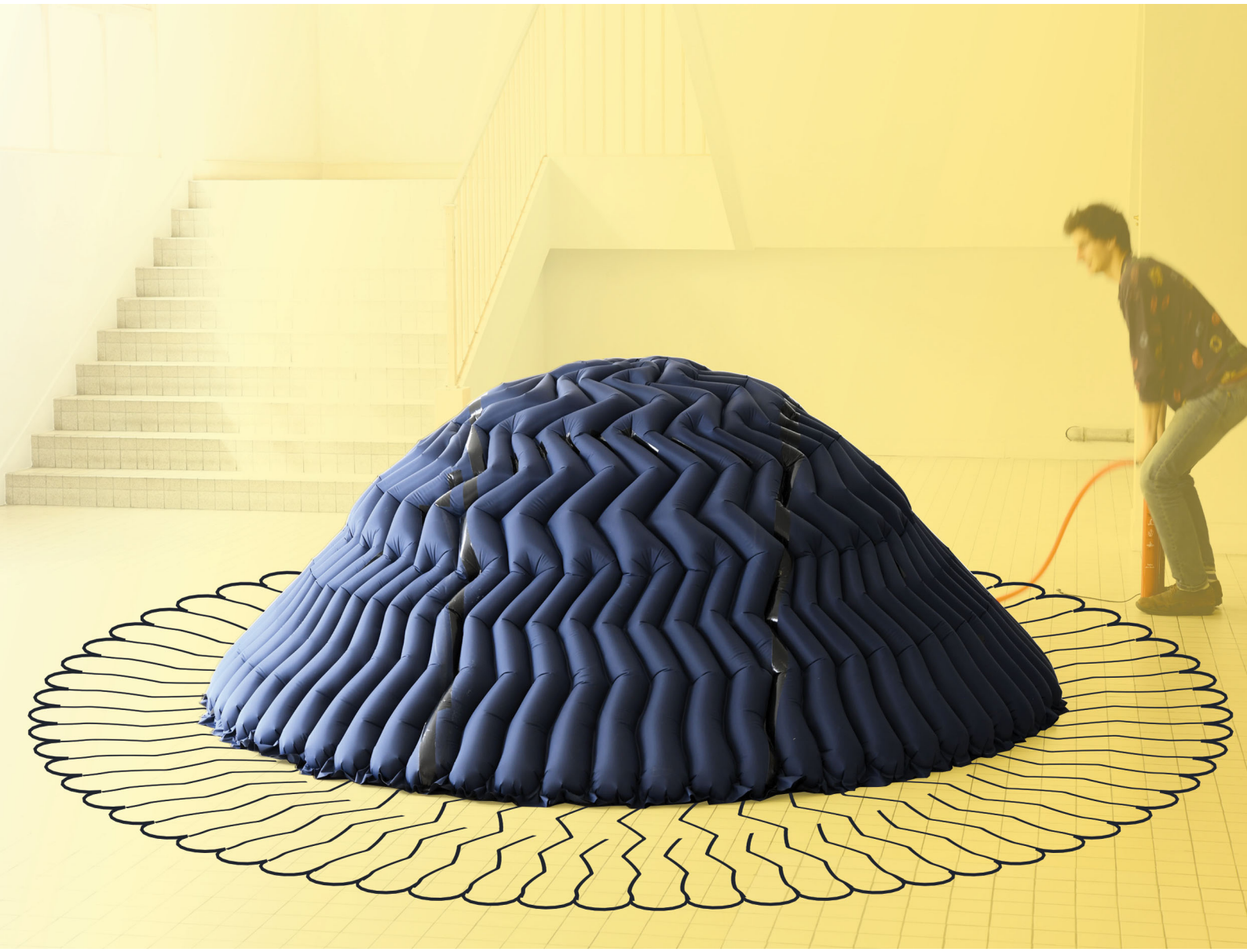

ISSN 1744-6848

ROYAL SOCIETY OF CHEMISTRY

PAPER
Emmanuel Siéfert, Benoît Roman *et al.*
Programming stiff inflatable shells from planar patterned fabrics

Soft Matter

PAPER

View Article Online
View Journal | View Issue

Cite this: *Soft Matter*, 2020, **16**, 7898

Programming stiff inflatable shells from planar patterned fabrics†

Emmanuel Siéfert, * Etienne Reyssat, José Bico and Benoît Roman *

Received 4th June 2020,
Accepted 16th July 2020

DOI: 10.1039/d0sm01041c

rsc.li/soft-matter-journal

Lack of stiffness often limits thin shape-shifting structures to small scales. The large in-plane transformations required to distort the metrics are indeed commonly achieved by using soft hydrogels or elastomers. We introduce here a versatile single-step method to shape-program stiff inflated structures, opening the door for numerous large scale applications, ranging from space deployable structures to emergency shelters. This technique relies on channel patterns obtained by heat-sealing superimposed flat quasi-inextensible fabric sheets. Inflating channels induces an anisotropic in-plane contraction and thus a possible change of Gaussian curvature. Seam lines, which act as a director field for the in-plane deformation, encode the shape of the deployed structure. We present three patterning methods to quantitatively and analytically program shells with non-Euclidean metrics. In addition to shapes, we describe with scaling laws the mechanical properties of the inflated structures. Large deployed structures can resist their weight, substantially broadening the palette of applications.

1 Introduction

As Carl Gauss demonstrated, curving a planar surface in two simultaneous directions requires changing the metrics, *i.e.* the distances between material points along the surface. Nature displays numerous examples of such shape changes induced by non-uniform growth, which for instance dictates the shape of plant leaves[1,2] or of our organs.[3] Bio-inspired shape shifting structures have been developed for applications in tissue engineering,[4] biomedicine[5] or drug delivery.[6] In order to achieve the metric distortion required for complex shape morphing, several actuation strategies have been intensively investigated in the last decade, ranging from swelling hydrogels,[7–10] liquid crystal elastomers[11,12] to, more recently, dielectric[13,14] or pneumatic[15] elastomers. These different solutions rely on basic scalar stimuli, respectively temperature, UV-light, electric field and pressure. However, their fabrication involves relatively complex processes: control of reticulation rate in hydrogels, precise control of the orientation of the nematic director field in liquid crystal elastomers, multi-layered electrodes for dielectric elastomers and precise 3D-printed molds for *baromorphs*. These objects are moreover inherently soft (Young modulus typically under 1 MPa), hindering applications to human size objects, architecture or space industry.

Other strategies to shape plates through a modification of the apparent metric without significantly stretching the material rely on cuts (kirigami),[16–18] folds (origami),[19,20] or internal hinges,[21] which allow for stiff materials to be used (*e.g.* polymers or even metals). Recently, pneumatic pressurization or vacuum have been introduced as a mean to actuate origami structures.[22–25] However, manufacturing still involves the complex folding of the structure prior to actuation. Despite recent advances, the actuation of folds remains indeed complex, prone to errors[26,27] and intrinsically soft.

Here, we present an alternative concept to transform initially flat sheets into stiff and lightweight inflatable shells (Fig. 1) using a versatile and scalable manufacturing technique:[28] two flat superimposed sheets (typically made of thermoplastic coated fabric) are heat-sealed together along seam lines. In contrast with mylar balloon structures where thin sheets are sealed along their edges,[29] locally parallel seam lines define here a network of channels over the whole area of the sheets (Fig. 2a, see ESI† and Supplementary movie 1 for details on the manufacturing). In-plane contractions distort metric in a non-Euclidean way, leading to the buckling of the structure into 3D shapes. This transformation is programmed by the specific pattern of the network. Inflation induces local bending of the sheets (Fig. 2b and c) and an apparent in-plane contraction perpendicular to the channels that we use as an average metric distortion.

In elegant *aeromorph* structures,[28] pressurized sheets with specific heat-sealed patterns fold into bistable soft hinges, programming essentially the extrinsic bending of the sheet rather than the intrinsic curvature (*i.e.*, the metric). Our proposed strategy is closer

PMMH, CNRS, ESPCI Paris, Université PSL, Sorbonne Université, Université de Paris, F-75005, Paris, France. E-mail: emmanuel.siefert@espci.fr, benoit.roman@espci.fr

† Electronic supplementary information (ESI) available. See DOI: 10.1039/d0sm01041c

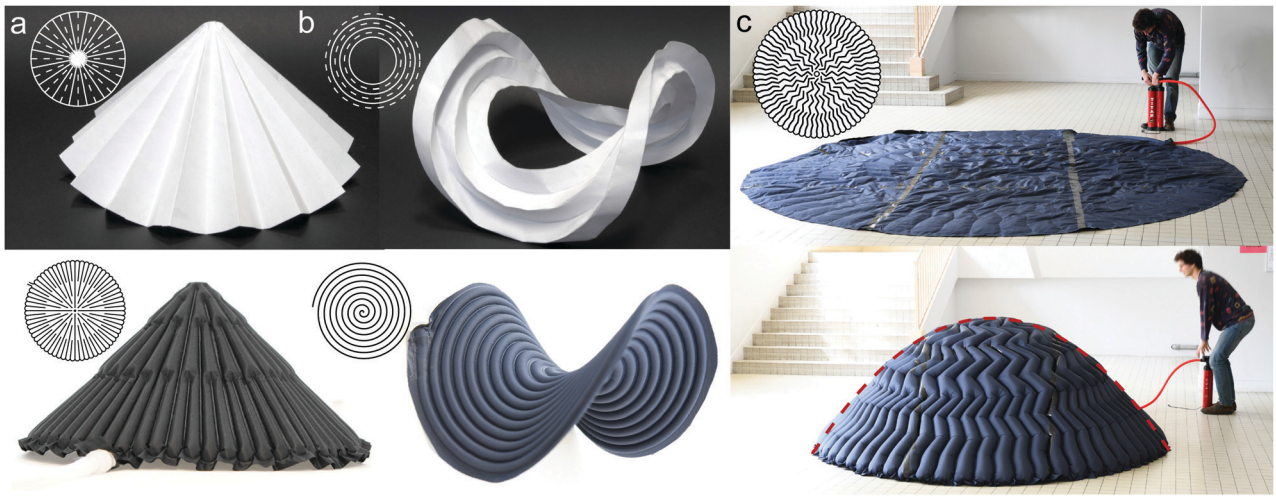

Fig. 1 Origami-inspired design of Gaussian morphing fabrics structures. (a) Paper origami cone made with alternate mountain (solid lines) and valley (dashed lines) radial folds. Inflated analogue composed of radial seams. (b) Concentric circular folds induce the formation of a saddle shape. The same anti-cone with seams along an Archimedean spiral. (c) A 3 m-wide and 1.2 m-high paraboloid structure with a Miura-ori type of pattern, fitting closely to the target shape (dashed line), sustains its own weight without any significant deflection.

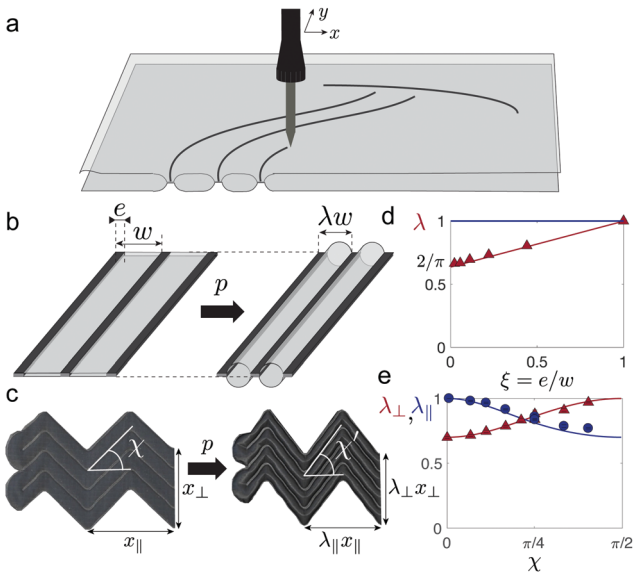

Fig. 2 In-plane metric distortion. (a) Two flat superimposed fabric sheets are heat-sealed along any desired path with a heating head mounted on an *XY*-plotter. (b) Upon inflation, the cross section between two locally parallel seams distant by w becomes circular, causing an in-plane contraction of magnitude $\lambda = 2/\pi$. (c) Varying the relative width $\xi = e/w$ of the seam line, homogenised contraction ratios ranging from $2/\pi$ to 1 can be obtained (red triangle: experiments; continuous line: model) (d), Deformation of inflated "zigzag" patterns inspired by miura-ori tessellation of incident angle χ. The orientation χ of the zigzags increases to a value χ' upon inflation. (e) Principal contraction ratios parallel (blue circles) and perpendicular (red triangles) to the average channel direction measured experimentally as a function of the zigzag angle χ. Solid lines correspond to the model (eqn (3) and (4)) with $\lambda = 0.7$.

to tessellated origami: seam lines are equivalent to the positions of valley folds, with mountain folds in between (Fig. 1a). As a simple example, radial folds in a paper disk lead to the formation of a cone. Similarly, an inflatable structure with radial seams morphs into a conical shape. Conversely, both origami with circular folds and its inflatable analogue with nearly azimuthal seams (Fig. 1b and Supplementary movie 2, ESI†) buckle into anti-cones.[30] Contrary to standard origami, the deployment of the 3D structure is here spontaneous upon inflation and does not require tedious mechanical actuation of individual folds. Moreover, rigidly and flat-foldable origami tessellations involve soft deployment modes, and cannot be stiff, whereas the effective folding angle in our inflatable structures, corresponding to the local contraction rate λ, is fixed by volume maximization in the highly bendable regime (Fig. 2b–e). The shape is obtained by the 2D patterning of flat sheets, not through the complex assembly of multiple patches, as in common inflatable structures.[31] Internal pressure p also provides stiffness to the resulting structure as in other large scale inflatables, such as fabric air beams,[32] stratospheric balloons[33] or even playground castles and architectural buildings.[34] We present and rationalize three different ways to distort the metrics and propose analytic procedures to program simple geometric shapes. We then discuss the mechanical properties of such Gaussian morphing fabric structures.

2 Patterning strategies and axisymmetric shape programming

In our approach, the pattern is locally made of parallel stripes of width w, with seam lines of width e (Fig. 2b). Upon inflation, the sheet bends perpendicularly to the seam lines to generate a tubular cross section for sufficiently large pressures ($p \gg Et^3/w^3$), where t is the thickness of the sheet and E its Young modulus. Owing to the quasi-inextensibility of the fabric sheets ($p \ll Et/w$), this change in cross section leads to an effective in-plane contraction perpendicular to the stripes. Taking the thickness e of the seam line into account (but neglecting

the effect of seam curvature[29]), the effective contraction factor reads:

$$\lambda(\xi) = \frac{2}{\pi}(1-\xi) + \xi \qquad (1)$$

where $\xi = e/w$ is the relative seam thickness, in very good agreement with experimental measurements (Fig. 2c). Conversely, no length change is observed along the seam lines. This direction may thus be seen as a director field for the anisotropic metric distortion of magnitude λ perpendicular and 1 parallel to the lines. Following the framework developed for liquid crystal elastomers,[11,12] the metrics of the inflated structure can be written as:

$$a(u,v) = R(\alpha(u,v))^t \begin{pmatrix} 1 & 0 \\ 0 & \lambda^2 \end{pmatrix} R(\alpha(u,v)) \qquad (2)$$

where (u,v) is a parametrization of the plane, α is the local angle of the director field, R the matrix of rotation and λ the contraction rate perpendicular to the channels. Interconnectivity between the channels is ensured by small apertures (smaller than the typical width w) at the ends of the seam lines, thus having limited influence on the local contraction governed by volume maximization. Note that in contrast to nematic elastomers, the contraction rate, λ can be varied in the range $[2/\pi,1]$ by tuning ξ. However, as the structure is symmetric through the thickness, the extrinsic curvature cannot be programmed.

We now illustrate how this metric distortion strategy can lead to a variety of stiff non-Euclidean shapes upon inflation. In the radial seam pattern shown in Fig. 1a, inflation induces a perimeter contraction of amplitude λ, which leads to the buckling of the disk into a cone of angle $2\arcsin\lambda$. In a nearly azimuthal pattern (archimedean spiral), radii are contracted by λ, and the structure buckles into an *anti-cone*[35] with an excess angle $2\pi(\lambda^{-1}-1)$ (Fig. 1b and Supplementary movie 2, ESI†). Both cone and anticone have a flat metric everywhere except at their apex, where Gaussian curvature is localized. General axisymmetric shapes with distributed Gaussian curvature are programmed by varying the angle α of seam lines with respect to the radial direction (Fig. 3a–d),[11,36] while keeping the seam width and thus the contraction λ nearly constant throughout the plane. As in liquid crystal elastomers,[11] the angle α fully determines the ratio of azimuthal *versus* radial contraction along the inflated shell. Arbitrary axisymmetric shapes, *e.g.* a paraboloid (Fig. 3b), or structures with constant negative Gaussian curvature (Fig. 3c) can be achieved (see ref. 36 for details on the programming procedure). The same method is applied in a cartesian coordinate frame[37] to program a helicoid of pitch $P = 4.5\ell$, where ℓ is the width of the deflated ribbon (Fig. 3d and

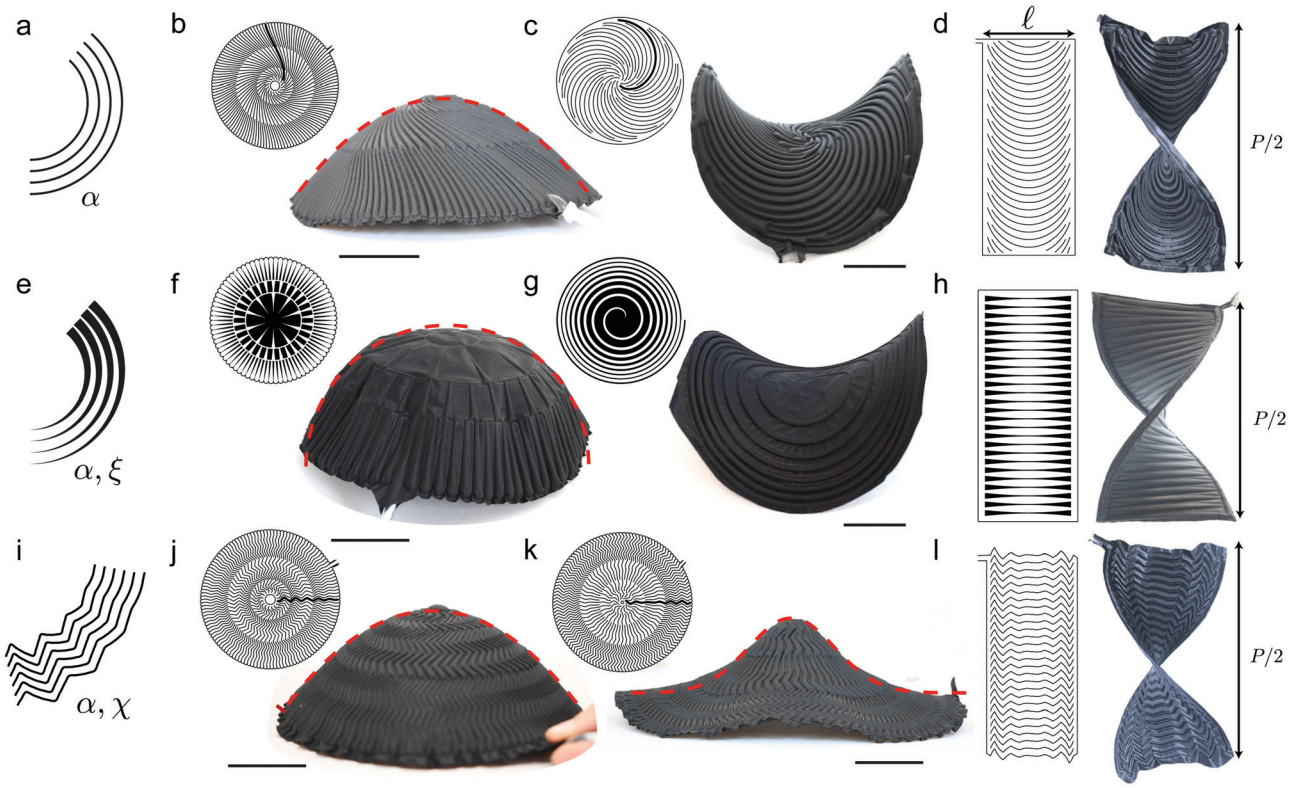

Fig. 3 Three metric distortion strategies. Simple geometric surfaces are programmed with corresponding seam patterns in insets. (a) Curved seam lines changing the orientation α of the in-plane contraction: (b) paraboloid, (c) saddle of constant negative Gaussian Curvature and (d) helicoid. (e) Variation of the contraction rate λ through the variation of the relative seam width ξ, in addition to the control of the orientation α of the seam: (f) hemisphere; (g) saddle; (h) helicoid. (i) Zigzag patterns with both the orientation α and the angle χ of the zigzags as degrees of freedom to distort the metric: (j) paraboloid, (k) Gaussian shape, (l) helicoid. For axisymmetric shapes, the red dashed lines correspond to the programmed target profiles. Each helicoid is programmed to make half a turn (pitch P twice longer than the inflated structure). Scale bars: 5 cm.

Supplementary movie 3, ESI†). More generally, the design of the director field can in principle be used to generate complex surfaces following the analogy with shape-programmed liquid crystal elastomers.[12,38]

Nevertheless, we may also take advantage of the possible variation of the contraction $\lambda \in [2/\pi,1]$ by adjusting the width of the seams (Fig. 3e), which offers an additional degree of freedom in the metric distortion and opens additional shape programming strategies. A hemisphere can for instance be programmed with radial seams of varying width, using eqn (1) and following the simple geometric rule $\lambda(r) = \frac{R}{r}\sin(r/R)$, where r is the radial coordinate in the flat state and R the programmed radius of curvature of the dome (Fig. 3f). The same method is applied with nearly azimuthal seams of decreasing width to program a saddle of constant negative Gaussian curvature (Fig. 3g and Supplementary movie 2, ESI†), or a helicoid with straight parallel seams (Fig. 3h and Supplementary movie 3 (ESI†); see ESI† for more details on the programming).

Another strategy to gain a second degree of freedom in the metric distortion is to design zigzag patterns that are reminiscent of *Miura-ori* origami tessellations. In addition to the main direction α of the channels, the characteristic angle χ of the zigzags (Fig. 2d) may be chosen. χ controls the ratio of the contractions $\lambda_\parallel$ and $\lambda_\perp$ respectively along and perpendicular to the average channel direction (Supplementary movie 4, ESI†). Inflating the structure induces a geometrical change from χ to $\chi' = \arctan(\tan\chi/\lambda)$. Using simple geometric considerations, we retrieve the average contraction rates:

$$\lambda_\parallel = \cos\chi'/\cos\chi = \frac{\lambda}{\sqrt{\sin^2\chi + \lambda^2\cos^2\chi}} \quad (3)$$

$$\lambda_\perp = \lambda\cos\chi/\cos\chi' = \sqrt{\sin^2\chi + \lambda^2\cos^2\chi} \quad (4)$$

which are in quantitative agreement with experimental measurements (Fig. 2e). Note that changing the angle χ of the zigzag does not impact the overall area contraction upon inflation, which remains equal to $\lambda = \lambda_\perp\lambda_\parallel$. Indeed, every air channel (from a zig or a zag) locally contracts uniaxially by an amount λ. Zigzag patterns can thus be viewed as a global isotropic area contraction followed by an in-plane shear varying both in direction (orientation α of the zigzag) and intensity (angle χ). Similarly to the computational techniques used with curved seams, zigzags (Fig. 3i) may be used to quantitatively program axisymmetric shapes (Fig. 3j, k and Supplementary movies 5,6, ESI†) or a helicoid (Fig. 3l and Supplementary movie 3, ESI†) (see ESI† for more details on the design of the seam networks). A study dedicated to the homogenization theory of zigzag patterns is under progress.

3 Stiffness of inflatable shells

Beyond geometry, such deployed structures are shells made of a collection of inflated beams and locally present highly anisotropic stiffness both for bending and stretching. In the regime of interest, the transverse bending stiffness per unit width of an array of parallel inflated beams scales as $B_\perp \sim Etw^2$, as in other inflatable structures.[32] Although $B_\perp$ barely depends on the applied pressure (as long as the air beam adopts the optimal circular section, *i.e.* $p \gg Et^3/w^3$), the maximum moment per unit width an array of beams can sustain without failing strongly depends on pressure[39–41] and typically scales as $pw^2 + Et^2$ (see ESI† for more details). Conversely, the bending stiffness along seam lines is proportional to Et^3 and is therefore orders of magnitude smaller than in the transverse direction: seams act as soft hinges between rigid inflated tubes. As a consequence, long straight seams favor floppy modes (*e.g.* the cone and the dome respectively illustrated in Fig. 1 and 3f bend easily along radial lines) whereas curved and narrow seams promote the global stiffness of the inflated structure. This strong stiffness anisotropy has a major impact on the shape selection among isometric embeddings of the target metrics: for instance, a helicoid (Fig. 3h) is selected rather than a catenoid, since it does not require the bending of the horizontal beams. Zigzag patterns appear as an interesting strategy to ensure the variation of the direction of the air beams at a mesoscale, while inducing stronger and more isotropic mechanical stiffness of the inflated structure. Since the envelope does not extend, the stretching modulus per unit width of pressurized patterns is related to variations of the enclosed volume and scales as pw in both directions (see ESI† for more details). Moreover, sharp changes in the direction of the seam induce, in the inflated state, compressive folds in the vicinity of the junctions between "zigs" and "zags".[29] In this region, the zigzaging beams may therefore deform through folding or unfolding the membrane without material strain. Upon bending, the curvature of such zigzag structures localizes at these softer spots. A kinking angle ϕ is achieved by the work $p\Delta V$ against the imposed pressure p, where the volume change ΔV is quadratic in ϕ. The localized linear hinge stiffness per unit width $C = p\partial^2(\Delta V)/\partial\phi^2$ is therefore proportional to p:

$$C = pw^2\mathscr{F}(\chi) \quad (5)$$

where w is the only local length scale and $\mathscr{F}$ a function of the zigzag angle χ. Experimental measurements using a three point bending test (Fig. 4a) are consistent with this prediction: C is linear with the pressure and appears independent of the sheet material properties.

Hinges can thus sustain a maximum moment that scales as pw^2 (as for straight beams). They also allow for much larger curvatures before an overall collapse, as many kinks are distributed over the structure. Hence, inserting hinge-like singularities typically reduces the local bending stiffness but also prevents the formation and localization of a single catastrophic kink in the structure. The global bending rigidity of zigzag patterns may be seen as a collection of beam components of stiffness $B_0 = Ew^2t/(4\pi)\cos^2\chi$ and hinges of rigidity C. The homogenized rigidity thus reads:

$$B_\perp = \left(B_0^{-1} + n_l C^{-1}\right)^{-1} \quad (6)$$

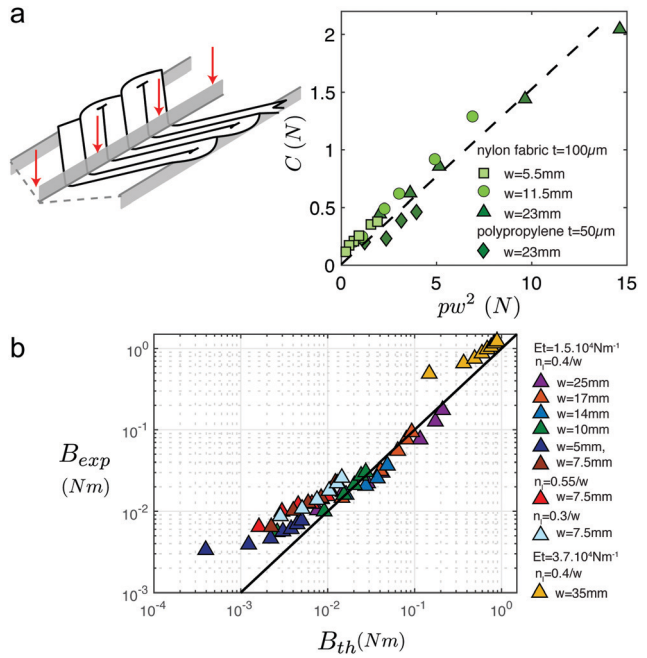

Fig. 4 Stiffness. (a) Inflated zigzag patterns bend preferentially along pseudo-hinges defined by junctions between zigs and zags. A three-point bending test provides measurements of the hinge stiffness resulting from volume variations. The hinge stiffness increases linearly with pressure. (b) Experimental value of the homogenized bending stiffness *versus* the prediction of the minimal model given by eqn (6).

where n_l is the number of direction changes per unit length. In the typical regime of interest, both terms are of the same order of magnitude and none may be neglected. Despite the strong simplifications implied in our description, eqn (6) provides a satisfying scaling law (using the prefactor found experimentally in Fig. 4a for C), especially at large enough pressures (where the assumption of circular cross section of the beams is verified).

All in all, the maximum moment per unit length the structure can sustain scales classically as pw^2. The typical maximum size of such inflatable structures $L_{\max}$ at which they can sustain their own weight scales thus as $L_{\max} \sim [pw^2/(\rho g t)]^{1/2}$. For typical values ($E \sim 10^9$ Pa, $w \sim 1$ m, $\rho \sim 10^3$ kg m^{-3}, $g \sim 10$ m s^{-2}, $t \sim 10^{-3}$ m and $p \sim 10^4$ Pa), $L_{\max}$ amounts to tens of meters. Architectural shape-morphing structures are thus reachable with this strategy. In order to highlight the high stiffness to weight ratio of such structures, a 4 m wide structure (3 m in the inflated state) has been manufactured using an ultrasonic sewing machine (Fig. 1c and Supplementary movie 7, ESI†).

4 Conclusion

Gaussian morphing fabrics constitute a versatile and simple technique to produce stiff shape-morphing pneumatic structures with well-defined programmable shapes. The manufacturing process is scalable and architectural size structures are within reach. Several patterning strategies – lines, seams of varying thickness and zigzags – have been introduced, allowing for one or two degrees of freedom in the metrics prescription. Although a wide variety of shapes can be programmed analytically, the general inverse problem, *i.e.* programming a pattern of seam lines such that the inflated structure deploys into a desired target shape, has to be solved numerically[12,38,42,43] and is beyond the scope of this article, since state-of-the-art techniques[12] fail due to the strong mechanical anisotropy of the structures.

Numerous extensions are possible for practical applications: several layers may be stacked with specific welding patterns between two consecutive fabric sheets, each pattern coding for one specific shape (Supplementary movie 8, ESI†). As the fabric used remains unstretched upon deployment, the structures may support metallic tracks for shape changing electronic devices.[44] Other actuation strategies may also be envisioned, such as hydrogel swelling inside the structure (Supplementary movie 9, ESI†). In order to bias the symmetry and promote a preferred deployment direction, fabric sheets of different thicknesses may finally be used. Altogether, our study offers a simple manufacturing platform where stiff shape-morphing structures are anticipated to find new innovative applications at human and architectural scale, ranging from rehabilitation medical tools to emergency shelters.

Conflicts of interest

There are no conflicts to declare.

Acknowledgements

We thank Tian Gao, Maïka Saint-Jean and Manon L'Estimé for technical help and Mark Pauly, Mark Warner, Julian Panetta and Antonio DeSimone for fruitful discussions. This work was supported by ANR SMArT (ANR-15-CE08-0007).

Notes and references

1 U. Nath, B. Crawford, R. Carpenter and E. Coen, *Science*, 2003, **299**, 1404.
2 A.-G. Rolland-Lagan, J. A. Bangham and E. Coen, *Nature*, 2003, **422**, 161–163.
3 T. Savin, N. A. Kurpios, A. E. Shyer, P. Florescu, H. Liang, L. Mahadevan and C. J. Tabin, *Nature*, 2011, **476**, 57–62.
4 B. Gao, Q. Yang, X. Zhao, G. Jin, Y. Ma and F. Xu, *Trends Biotechnol.*, 2016, **34**, 746–756.
5 M. Cianchetti, C. Laschi, A. Menciassi and P. Dario, *Nat. Rev. Mater.*, 2018, **3**, 143.
6 M. Sitti, *Nat. Rev. Mater.*, 2018, **3**, 74.
7 Y. Klein, E. Efrati and E. Sharon, *Science*, 2007, **315**, 1116–1120.
8 J. Kim, J. A. Hanna, M. Byun, C. D. Santangelo and R. C. Hayward, *Science*, 2012, **335**, 1201–1205.
9 R. M. Erb, J. S. Sander, R. Grisch and A. R. Studart, *Nat. Commun.*, 2013, **4**, 1712.
10 A. S. Gladman, E. A. Matsumoto, R. G. Nuzzo, L. Mahadevan and J. A. Lewis, *Nat. Mater.*, 2016, **15**, 413–418.
11 M. Warner, *Annu. Rev. Condens. Matter Phys.*, 2020, **11**, 125–145.

12 H. Aharoni, Y. Xia, X. Zhang, R. D. Kamien and S. Yang, *Proc. Natl. Acad. Sci. U. S. A.*, 2018, **115**, 7206–7211.
13 H. Bense, M. Trejo, E. Reyssat, J. Bico and B. Roman, *Soft Matter*, 2017, **13**, 2876–2885.
14 E. Hajiesmaili and D. R. Clarke, *Nat. Commun.*, 2019, **10**, 183.
15 E. Siéfert, E. Reyssat, J. Bico and B. Roman, *Nat. Mater.*, 2019, **18**, 24.
16 M. A. Dias, M. P. McCarron, D. Rayneau-Kirkhope, P. Z. Hanakata, D. K. Campbell, H. S. Park and D. P. Holmes, *Soft Matter*, 2017, **13**, 9087–9092.
17 T. Castle, Y. Cho, X. Gong, E. Jung, D. M. Sussman, S. Yang and R. D. Kamien, *Phys. Rev. Lett.*, 2014, **113**, 245502.
18 D. M. Sussman, Y. Cho, T. Castle, X. Gong, E. Jung, S. Yang and R. D. Kamien, *Proc. Natl. Acad. Sci. U. S. A.*, 2015, **112**, 7449–7453.
19 L. H. Dudte, E. Vouga, T. Tachi and L. Mahadevan, *Nat. Mater.*, 2016, **15**, 583.
20 Y. Zhao, Y. Endo, Y. Kanamori and J. Mitani, *J. Comput. Des. Eng.*, 2018, **5**, 442–448.
21 R. Guseinov, C. McMahan, J. Pérez, C. Daraio and B. Bickel, *Nat. Commun.*, 2020, **11**, 1–7.
22 R. V. Martinez, C. R. Fish, X. Chen and G. M. Whitesides, *Adv. Funct. Mater.*, 2012, **22**, 1376–1384.
23 J. T. Overvelde, T. A. De Jong, Y. Shevchenko, S. A. Becerra, G. M. Whitesides, J. C. Weaver, C. Hoberman and K. Bertoldi, *Nat. Commun.*, 2016, **7**, 10929.
24 S. Li, D. M. Vogt, D. Rus and R. J. Wood, *Proc. Natl. Acad. Sci. U. S. A.*, 2017, **114**, 13132–13137.
25 W. Kim, J. Byun, J.-K. Kim, W.-Y. Choi, K. Jakobsen, J. Jakobsen, D.-Y. Lee and K.-J. Cho, *Sci. Rob.*, 2019, **4**(36), eaay3493.
26 J.-H. Na, A. A. Evans, J. Bae, M. C. Chiappelli, C. D. Santangelo, R. J. Lang, T. C. Hull and R. C. Hayward, *Adv. Mater.*, 2015, **27**, 79–85.
27 M. Z. Miskin, K. J. Dorsey, B. Bircan, Y. Han, D. A. Muller, P. L. McEuen and I. Cohen, *Proc. Natl. Acad. Sci. U. S. A.*, 2018, **115**, 466–470.
28 J. Ou, M. Skouras, N. Vlavianos, F. Heibeck, C.-Y. Cheng, J. Peters and H. Ishii, Proceedings of the 29th Annual Symposium on User Interface Software and Technology, 2016, pp. 121–132.
29 E. Siéfert, E. Reyssat, J. Bico and B. Roman, *Proc. Natl. Acad. Sci. U. S. A.*, 2019, **116**, 16692–16696.
30 M. Dias, L. Dudte, L. Mahadevan and C. Santangelo, *Phys. Rev. Lett.*, 2012, **109**, 114301.
31 M. Skouras, B. Thomaszewski, P. Kaufmann, A. Garg, B. Bickel, E. Grinspun and M. Gross, *ACM Trans. Graph.*, 2014, **33**, 63:1–63:10.
32 R. Comer and S. Levy, *AIAA J.*, 1963, **1**, 1652–1655.
33 M. Pagitz, *Philos. Trans. R. Soc., A*, 2007, **365**, 3003–3017.
34 T. Herzog, *Pneumatic Structures: a hanbook of inflatable architecture*, Oxford University Press, 1976.
35 J. Dervaux and M. Ben Amar, *Phys. Rev. Lett.*, 2008, **101**, 068101.
36 E. Siéfert and M. Warner, *Proc. R. Soc. A*, 2020, DOI: 10.1098/rspa.2020.0047.
37 H. Aharoni, E. Sharon and R. Kupferman, *Phys. Rev. Lett.*, 2014, **113**, 257801.
38 I. Griniasty, H. Aharoni and E. Efrati, *Phys. Rev. Lett.*, 2019, **123**, 127801.
39 C. R. Calladine, *Theory of shell structures*, Cambridge University Press, 1989.
40 P. Seide and V. Weingarten, *J. Appl. Mech.*, 1961, **28**, 112–116.
41 J. Guo, C. Wang, J. Zhang and Q. Tao, *J. Spacecr. Rockets*, 2020, 1–4.
42 M. Konaković, K. Crane, B. Deng, S. Bouaziz, D. Piker and M. Pauly, *ACM Trans. Graph.*, 2016, **35**, 1–11.
43 J. W. Boley, W. M. van Rees, C. Lissandrello, M. N. Horenstein, R. L. Truby, A. Kotikian, J. A. Lewis and L. Mahadevan, *Proc. Natl. Acad. Sci. U. S. A.*, 2019, **116**, 20856–20862.
44 J. A. Rogers, T. Someya and Y. Huang, *Science*, 2010, **327**, 1603–1607.